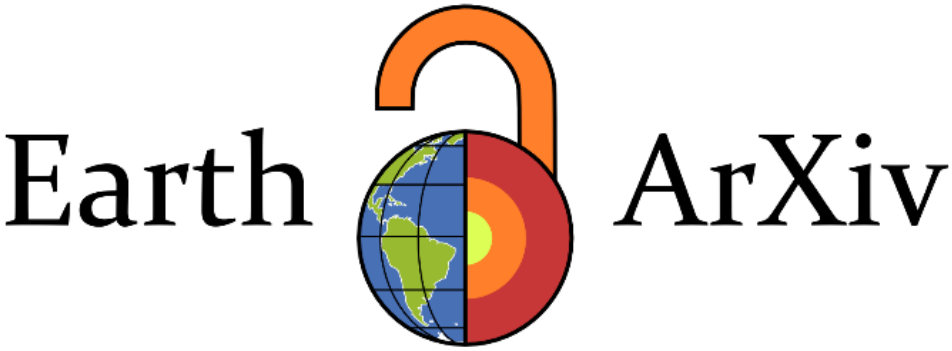

Earthquake Swarm in Santorini - Greece: Recurrence Quantification Analysis and Investigation of Causal Relationship with Tidal Forces

S. Maltezos*[a] and A. Georgakopoulou[a]

[a]*National Technical University of Athens, Department of Physics, 15780 Athens, Greece*

Abstract

Abstract. In early 2025, an unusual earthquake swarm initiated in the sea area of the small uninhabited islet Anydros between Santorini and Amorgos islands in Greece. The unusual nature of this seismic activity and its subsequent seismic follow-up, motivated us to study its dynamical and statistical features. Namely, we investigated for a potential causal relationship between a simple model regarding normal component of tidal forces caused by Moon and Sun and the dynamical evolution of this earthquake swarm in this area within the same time period. We have faced this problem deeply applying three methods suitable for understanding this overall seismic activity: the Recurrence Quantification Analysis, with the associated metrics, referring to identify similar states of complex dynamic systems, the linear Granger causality Test and the Convergent Cross Mapping used in for the reconstruction of embedded phase space. Beside the individual results, we have combined them in synergy to obtain a robust concluding result. Moreover, in the same context of investigating causality, we have performed a global statistical study regarding the probability for triggering strong earthquakes, in the highest magnitude range from M6.0 and above, within narrow or wider time slices around the four Moon phases. A modeling of the overall probability density function is also given.

Keywords— Earthquake swarm, Tidal triggering, Recurrence Plots, Causality, Granger Test, Convergent Cross Mapping

1 Introduction

Earthquake swarms (or seismic swarms) are an unusual but interesting phenomenon that has been observed in various regions of Earth planet. A notable seismic activity (earthquake swarm and the subsequent aftershock) has been take place in the extended region around Anydros, a small uninhabited islet located northeast of Santorini and southwest of Amorgos in the southern Aegean Sea, mainly started by the end of January 2025. According to data from the Institute of Geodynamics - National Observatory of Athens, during the period from 24/01/2025 to 06/03/2025, a total of 4062 seismic events have been analyzed [1]. Preliminary interpretations suggest that the swarm may be linked to tectonic stress redistribution or magmatic processes beneath the Santorini volcanic complex. However, geodetic data have not yet indicated any substantial ground deformation, and there is currently no evidence of imminent volcanic activity. In Fig. 1 a geographical visualization of the earthquake swarm in the region of Santorini and Amorgos islands is illustrated together with the earthquake epicenters. Although, in this seismic activity, the earthquake magnitudes were relatively small, with mean value about $M_{\mathrm{L}}3.0$ (local magnitude) during the first two-weeks phase becoming even less later down to the level of $M_{\mathrm{L}}2.0$. The daily event rate was accordingly very high and decreasing progressively, associated with intrinsic statistical fluctuations.

The peculiarity and unusual nature of this geological and seismologic phenomenon had challenged us to study the overall characteristics of the associated complex underlying system, both statistically

*Corresponding author: S. Maltezos, National Technical University of Athens, 15780 Athens, Greece, e-mail: maltezos@central.ntua.gr

and in terms of its dynamical behavior [2], [3]. In addition, we wanted to study and investigate a potential causal relationship between the daily time series of the Lunar and Solar tidal forces (as the cause) and the daily rate of seismic events (as the effect) at the same time period. The tidal forces are studied by researchers whether could act to such an extent that they can trigger geological movements in the grid of existing faults.

The present work is organized as follows. After the introduction (Section 1), in Section 2,the motivation for our study is explained. In Section 3 we present the theoretical approach of the recurrence times as well as its application in the time series under study. In Section 4 the investigation methods of causal relationship are described and implemented while in Section 5 the evaluation of the results are presented together with a global statistical study of earthquakes. Finally, the conclusions are discussed.

2 Motivation for studying the earthquake triggering

2.1 Brief historical overview

The idea that tidal forces—gravitational influences, primarily from the Moon and the Sun, could trigger the seismic activity has intrigued scientists for over a century. As early as the late 19^{th} and early 20^{th} centuries, researchers began to explore potential correlations between tidal stresses and earthquake occurrences, though the tools and data available were limited.

In the 1960's and 1970's, with the advent of more precise seismological instruments and a growing global earthquake catalog, interest in this topic revived. Researchers began statistically analyzing whether earthquakes or earthquake swarms, were more likely to occur during specific phases of the Earth tide cycle (e.g., at times of peak tidal stress) and perhaps might be driven by them.

During the 1980's and 1990's, several studies suggested weak but statistically significant correlations between Earth tides and shallow thrust or normal faulting events. However, the results were often inconsistent and varied depending on tectonic setting, depth, and magnitude. In the 2000's and 2010's, more refined models of tidal stress and access to massive earthquake datasets enabled more sophisticated analyses. Some studies reported that earthquakes near critical stress conditions could be triggered by small additional stresses from tides, particularly in volcanic or geothermal regions where earthquake swarms are common. There were also indications that large mega thrust earthquakes, such as those in subduction zones, might show a weak preference for occurring at certain tidal phases. Despite these findings, a definitive causal relationship remains elusive.

Most researchers agree that while tidal forces can modulate the timing of earthquakes under specific conditions, they are not a primary cause. The prevailing view is that tidal stress might "nudge" a fault that is already close to failure, acting as a triggering mechanism rather than a root cause. Today, the topic remains an active area of research, with ongoing studies combining seismology, geophysics, and statistical modeling to better understand the complex interplay between external forces and tectonic stress accumulation.

2.2 Potential cause of triggering by tidal forces

Most research on tidal triggering of seismic events has relied on statistical correlation methods, such as the Schuster Test and its extension, Schuster Spectrum [4], to assess the relationship between tidal phases and earthquake occurrences. For instance, studies have observed correlations between Earth tides and earthquake occurrences in various regions, including Japan, Taiwan, and Colombia. These studies suggest that tidal forces may influence seismic activity, particularly in areas with specific tectonic settings [5], [6]. Moreover, a characteristic pattern in the long-term variation of radon concentrations in soil has been observed, which seems to be associated with the variation of regional stress in relation to seismicity. Changes in noble radioactive gas Radon concentration levels begin before rock rupture and therefore before the earthquake occurs [7].

In an earlier study conducted researchers investigated to approximately 12.000 earthquakes recorded in 9 distinct seismogenic areas across Italy between 2005 and 2011 [8]. Benford's Law of first digit distribution (BL) [9], [10], [11], [12] was selected and applied because inter-event times in seismic

sequences might follow multiplicative, scale-invariant processes. The analysis, focused specifically on earthquakes with magnitudes typically greater or equal than $M_{\mathrm{L}}3.0$ that had formed clusters of at least 30 daily events. Briefly, their hypothesis was that deviations from the BL could indicate external factors influencing seismicity, particularly the Earth tidal forces. Consistently with prior research ([13] and [14]), their findings demonstrated that recurrence intervals between consecutive seismic events aligned closely with BL distribution.

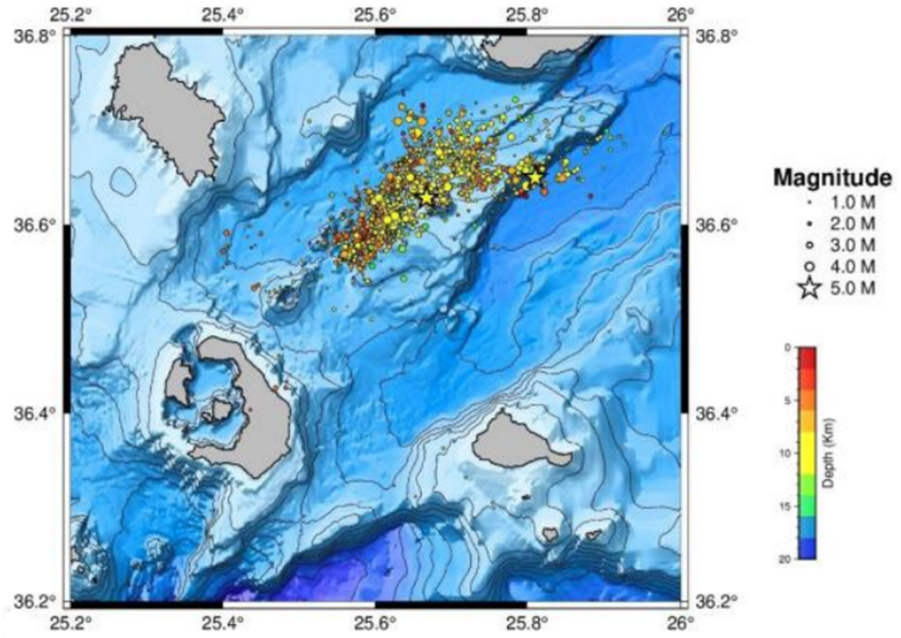

Figure 1: An indicative seismic swarm visualization showing the seismic events between Santorini and Amorgos islands, recorded from January 24 to March 6, 2025. The color scale is related to the event depths. This image been obtained from the reference [1].

Significant deviations emerged when analyzing intervals between non-consecutive seismic events, notably correlated with tidal frequencies such as ter-diurnal and quasi-diurnal cycles. These results indicated a potential modulation of seismic activity by tidal forces, particularly evident around periods of full and new Moon phases. Such insights offer promising implications for earthquake forecasting and hazard assessment.

However, in the present work, at one hand, we are concentrated to a smaller spacial region of seismic activity deployed as an autonomous event allowing us for a reliable statistical analysis, and on the other hand, we investigated the casual relationship based on advanced methods described in the next and by using the Matlab Framework [15]. We must notice that in this case the interaction among the individual geological faults is happened almost instantaneously due to the small distances between each other. Moreover, the long-term duration of this activity (a few months) gave us to collect the required number of data for higher accuracy of causality investigation.

Given the potential of statistical methods to uncover causal relationships in complex systems, applying these methods to the study of tidal triggering of earthquakes could provide deeper insights. However, such applications would require high-resolution, long-term datasets and careful consideration of the underlying assumptions of these methods.

2.3 Model of the tidal forces

Given the important feature of this seismic activity, that it has been started abruptly as usually happens in single earthquakes followed by a seismic sequence, a fact which may refer to the most likely and fundamental triggering cause which is a phase synchronization of the tidal forces. In order to study a potential triggering of this seismic event, we investigated an appropriate, but simplified diurnal model, of the tidal forces in the region around Anydros island (Lat: 36.842$^{\mathrm{o}}$ N, Lon: 25.955$^{\mathrm{o}}$

E) caused by the Moon and Sun combined together during the year. The total tidal force model that we use in the present study is the following

$$F_t = F_0 + A_{\rm M}\cos(\omega_{\rm M}t + \phi_{\rm M}) + A_{\rm S}\cos(\omega_{\rm S}t + \phi_{\rm S}) + A_{\rm m}\cos(\omega_{\rm m}t + \phi_{\rm m}) + A_{\rm y}\cos(\omega_{\rm y}t + \phi_{\rm y}) \qquad (2.1)$$

where F_t is the total force per unit mass, while F_0 is a constant baseline force. Also, A_M and A_S are the amplitudes of the periodical variable contributions of the Moon and Sun, A_m and A_y are the contributions of the monthly and yearly cycle. ω_M, ω_S denote the angular velocities of the Moon and Sun, respectively and $\omega_{\rm m}$, $\omega_{\rm y}$ are the monthly and yearly component, respectively. The Moon phases ϕ depend on the position of the Moon and Sun versus time [16],[17]. The values of the parameters used in the tidal force model are given in Table 2.

Component	**Period**	**Phase (typical values in Aegean)**
Main Moon (M2)	12.42 hours	$\phi_M \approx 30^\circ - 60^\circ$
Main Sun (S2)	12.00 hours	$\phi_S \approx 20^\circ - 50^\circ$
Monthly (Mm)	29.53 hours	$\phi_{\rm m} \approx 10^\circ - 30^\circ$
Yearly (Sy)	365.25 days	$\phi_{\rm y} \approx 5^\circ - 20^\circ$

Table 1: Periods and phases for the components used in the tidal model.

Amplitude $\times 10^6$ [N kg^{-1}]	**Angular velocity** [rad $\cdot$ day^{-1}]	**Phase** [^{o}]
$A_{\rm M} = 1.00$	$\omega_{\rm M} = 2\pi/12.42$	$\phi_{\rm M} = 45$
$A_{\rm S} = 0.50$	$\omega_{\rm S} = 2\pi/12.00$	$\phi_{\rm S} = 30$
$A_{\rm m} = 0.30$	$\omega_{\rm m} = 2\pi/29.53$	$\phi_{\rm m} = 15$
$A_{\rm y} = 0.02$	$\omega_{\rm y} = 2\pi/365.25$	$\phi_{\rm y} = 10$

Table 2: The values of the parameters that we have used in the tidal force model.

For more generic tidal phenomena, mainly in oceans, the TPXO models and the OTPS (Oregon State University Tidal Prediction Software) are essential tools. The values for the various phases that we have used in the above simple model are presented in Table I 1. The plots of the tidal model forces and the earthquake daily rate during the first four months of 2025 are shown in Fig. 8. The minima in the tidal force plot correspond to full moon and new moon phase (the deeper ones) while the maxima to the full crescent moon. The earthquake data obtained from the Institute of Geodynamics – National Observatory of Athens (NOA) [18] and further processed. The abrupt increase of the earthquake daily rate occurred at February 1, that is 3 days after new Moon phase.

For the present overall investigation, the selected geographic region was bounded from Latitude 36.4$^{\rm o}$ to 36.8$^{\rm o}$ and from Longitude 25.4$^{\rm o}$ to 26.0$^{\rm o}$.

3 Approach by using recurrence plots

Recurrence is a fundamental property of dynamical systems, which can be exploited to characterize the system's behavior in phase space. A powerful tool for their visualization and analysis called recurrence plot (RP) was introduced in the late 1980's [19]. The formal concept of recurrences was introduced by Henri Poincaré in his seminal work from 1890, for which he won a prize sponsored by King Oscar II of Sweden and Norway on the occasion of his majesty's 60th birthday [20]. In 1987, Eckmann et al. introduced the so-called Visual Recurrence Analysis (VRA) based on a graphical method designed to locate hidden recurrent patterns observed in the phase space dynamical systems, while the RP is used to visualize the recurrences of dynamical systems [21]. Suppose we have a trajectory $\{\vec{x}_i\}_{i=1}^N$ of a system in its phase space. The components of these vectors could be various variables e.g., as temperature, air pressure, humidity and many others. In our case the time series is the earthquake magnitude. The development of the systems is then described by a time series of these vectors, representing a trajectory in an abstract mathematical space. The corresponding RP is based on the following recurrence matrix

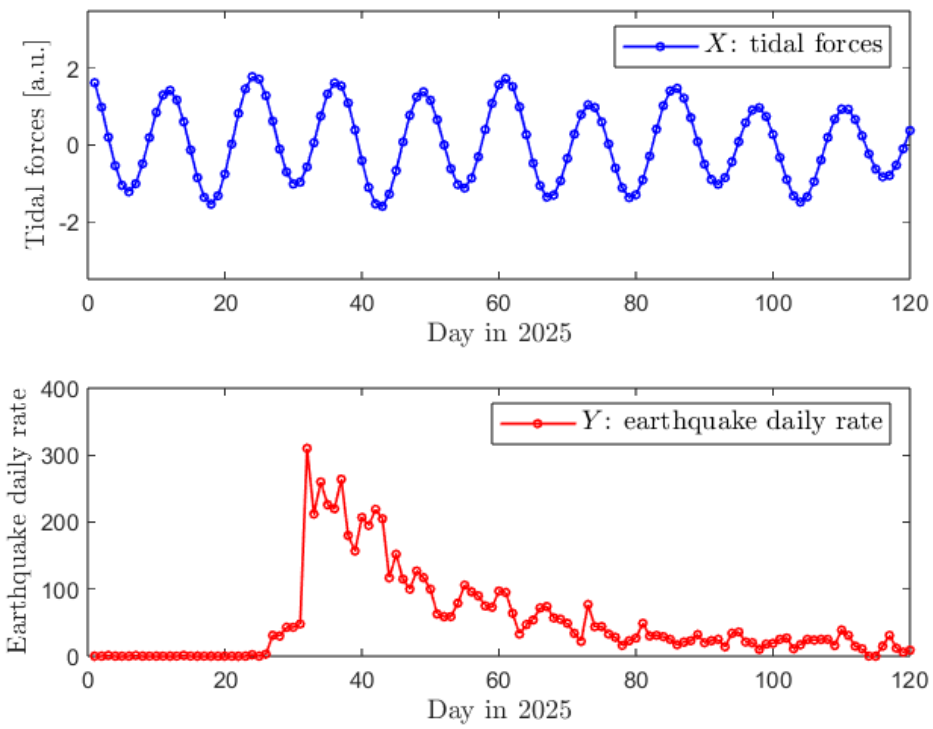

Figure 2: Plot of the two time series during the first four months of 2025. Upper plot: the normal component of the tidal force, where the positive values correspond to the tidal forces in a direction from the ground outwards(tides), while the negative ones correspond to the opposite directions (ebb). The first minimum corresponds to the New Moon phase and the next extremes represent to the First Quarter, Full Moon and the Last Quarter, respectively. Lower plot: the daily rate of earthquakes in the region around Anydros island.

$$\mathbf{R}_{i,j} = \begin{cases} 1, & \bar{x}_i \approx \bar{x}_j, \\ 0, & \bar{x}_i \not\approx \bar{x}_j, \end{cases} \quad i,j = 1,\ldots,N. \tag{3.1}$$

where N is the number of considered states and $\vec{x}_i\} \approx \vec{x}_j$ means equality up to an error (or distance) ε. Note that this error is essential as systems often do not recur exactly to a formerly visited state but just approximately. Roughly speaking, the matrix compares the states of a system at times i and j. If the states are similar, this is indicated by a one in the matrix, i.e. $\mathbf{R}_{i,j} = 1$. If on the other hand the states are rather different, the corresponding entry in the matrix is $\mathbf{R}_{i,j} = 0$.

The RP efficiently visualizes recurrences and can be formally expressed by the matrix

$$\mathbf{RP}_{i,j}(\varepsilon) = \Theta\left(\varepsilon - \| \vec{x_i} - \vec{x_j} \|\right), \quad i,j = 1,\ldots,N. \tag{3.2}$$

where where N is the number of measured points $\vec{x_i}$, ε is a threshold distance, $\Theta(\cdot)$ is the Heaviside function and $\|\cdot\|$ is the norm.

The selection of the parameter threshold distance ε is crucial for a RP. Special attention has to be paid for its choice. If it is chosen too small, there may be almost no recurrence points and we cannot learn anything about the recurrence structure of the underlying system. On the other hand, if it is chosen too large, almost every point is a neighbor of every other point, which leads to a lot of artifacts. A too large value includes also points into the neighborhood which are simple consecutive points on the trajectory. This effect is called tangential motion and causes thicker and longer diagonal structures in the RP as they actually are. Hence, we have to find a compromise value of ε.

So the matrix tells us when similar states of the underlying system occur. This Eckmann's report shows that much more can be concluded from the recurrence matrix. The patterns of recurrences

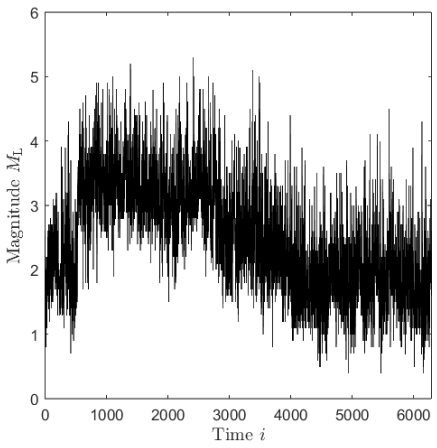

Figure 3: Plot of the magnitudes of earthquake swarm during January, February, March and April of 2025 (120 days in total). The discrete time of the time series is used.

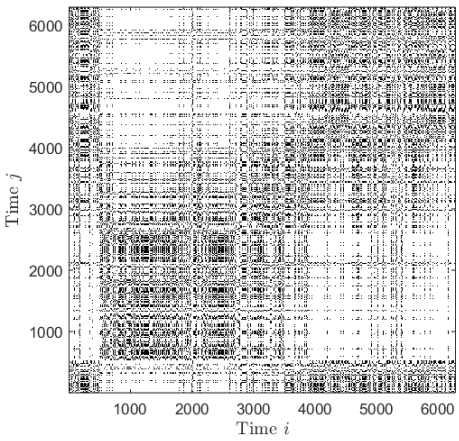

Figure 4: Plot of the recurrence plot (RP) of the earthquake magnitudes time series with distance threshold $\varepsilon = 0.3$. A Drift type structure of non-stationary dynamical system is observed.

allow studying dynamical systems and their trajectories. A scientific work measures of complexity based on recurrence plots are introduced, which allow to identify laminar states and their transitions to regular as well as other chaotic regimes in complex systems. These measures make the investigation of intermittency of processes possible, even if they are only represented by short and nonstationary data series [22], [23], [24], [25].

This method has been applied to the present work with the aim of characterizing the time series, both in terms of earthquake magnitudes and in terms of the evolution of the phenomenon of seismic activity. In Figs. 3 and 4 the time series of earthquake magnitudes and the obtained RP are presented, respectively. For ε we have chosen a value of 0.5 which correspond to about 10% of the maximum spread of the earthquake magnitudes. Before constructing the RP of the time series under study, we have analyzed the time series we have estimated the optimum embedding dimension, E, of the reconstructed phase space as well as the time delay (lag), τ (see more in Section 4.3). These parameters, together with ε, are indispensable and crucial in this analysis.

In the RP (shown Fig. 4) we give a qualitative interpretation below by using $E = 2$ and $\tau = 6$:

1. *Non-random, structured recurrence patterns*: the presence of repeated diagonal structures (without complete regularity) suggests that the seismic magnitudes are not random, but exhibit some dynamic dependence or recursion. This is consistent with swarms, which are characterized by earthquakes with similar characteristics (e.g. magnitudes, location) and non-ergodic evolution in time.

2. *Short and broken diagonal lines*: it reflects a form of intermittent determinism and it is frequently interrupted by irregular or chaotic phases — a behavior typical of complex systems such as those governed by frictional fault mechanics or stress transfer.

3. *Sparse and dense regions*: Contains alternating regions of high and low recurrence density, likely correspond to phases of intense seismic activity (with recurring magnitude patterns) and quiescence or transition, respectively. This implies non-stationary process, which is a hallmark of swarm-type behavior.

4. *Lack of strict periodicity*: The RP lacks long, uninterrupted diagonal lines suggesting that the system does not evolve through strict periodic processes but instead exhibits quasi-periodic or chaotic behavior, consistent with the idea of self-organized criticality (SOC) often proposed for seismic swarms.

Performing the "Recurrence Quantification Analysis" (RQA) [26], [27] which is used to analyze and quantify the dynamics of time series, based on the recurrence of data in the spectrum of the phase

spectrum we obtained the metrics given below. The range of the vale is shown in brackets while N concerns length of the time series ($N = 6292$ in this case):

- Recurrence Rate (RR)=0.074 [0,1], the seismic activity has fewer repeated patterns, or less self-similarity over time.
- Determinism (DET)=0.27 [0,1], moderate level of determinism, meaning that there are some predictable fluctuations in the seismic activity, but it is not fully deterministic.
- Laminarity (LAM)=0.40 [0,1], there are areas with relatively smooth or less fluctuations in the seismic activity.
- Entropy (ENT)=0.56 [1,∞], there is some uncertainty in the evolution of the seismic activity, but it is not completely chaotic.
- Longest Diagonal Line (Lmax)=6288 [1,N], this high value indicates that there are long periods of repeated structure or trends in the seismic activity.
- Trapping Time (TT)=2.43 [1,N], the seismic activities remain in specific states for a moderate amount of time.

Another possibility to compare different systems is to consider the recurrences of their trajectories in their respective phase spaces separately and look for the times when both of them recur simultaneously, i.e. when a joint recurrence occurs. By means of this approach, the individual phase spaces of both systems are preserved. Formally, this corresponds to an extension of the phase space to $\mathbb{R}^{d_x+d_y}$, where d_x and d_y are the phase space dimensions of the corresponding systems, which are in general different (i.e. it corresponds to the direct product of the individual phase spaces). Furthermore, two different thresholds for each system, $\varepsilon^{\vec{x}}$ and $\varepsilon^{\vec{y}}$, are considered while the criteria for choosing set separately according to the natural measure of each system. Therefore, by the bi-variate extension a Joint Recurrence Plot (JRP) allows studying the relationship between two different systems by examining the occurrence of similar states. The JRP is essentially the *Hadamard product* of the recurrence plot of the first system and the recurrence plot of the second system.

Based on this idea, the *Joint Recurrence Matrix* for two systems $\vec{x}$ and $\vec{y}$ is expressed as follows

$$\mathbf{JR}_{i,j}^{\vec{x},\vec{y}}\left(\varepsilon^{\vec{x}},\varepsilon^{\vec{y}}\right)=\Theta\left(\varepsilon^{\vec{x}}-\parallel\vec{x_i}-\vec{x_j}\parallel\right)\Theta\left(\varepsilon^{\vec{y}}-\parallel\vec{y_i}-\vec{y_j}\parallel\right),\quad i,j=1,\ldots,N. \tag{3.3}$$

The graphical representation of the matrix $\mathbf{JR}_{i,j}$ is called *JRP*. The definition of the RP is a special case of the definition of the JRP for only one system.

In our study we have also implemented the JR matrix for the two time series originated from two different dynamical systems: that of the model of the tidal forces and that of the earthquake daily rate in the same time period of the four months of 2025.

The RP of the tidal model forces and that of the earthquake daily rate are presented in Figs. 5 and 6, respectively. The first refers to periodic (super-positioned harmonic oscillations). The threshold distance used was equal to 0.34. Regarding the structure of the second RP, we can give the following qualitative interpretation

1. *Block-like patterns and segmentation*: reveals distinct square and rectangular blocks of recurrence. This suggests the presence distinct seismic regimes with internal similarity.
2. *Sparse recurrence across regimes*: between these blocks, recurrence points are sparse, indicating that the system does not revisit prior states once it transitions, reflecting a tectonic segment shifting from swarm to quiescence. The diagonal gap or thinning in the middle may reflect a change in seismic behavior being more chaotic.
3. *Vertical and horizontal line structures*: Recurrent vertical and horizontal lines (mainly the bottom-right quadrant) suggest laminar phases, possibly indicating stress accumulation or inhibited rupture propagation.

Performing the RQA, where $N = 120$ in this case and by using $\varepsilon = 1$, $E = 2$ and $\tau = 4$, we obtain the following Metrics:

- Recurrence Rate (RR)=0.52, low recurrences indicating chaotic behavior.
- Determinism (DET)=0.97, the system follows defined patterns.
- Laminarity (LAM)=0.98, stable behavior with a some degree of periodicity.
- Entropy (ENT)=3.0, a level of complexity or disorder.
- Longest Diagonal Line (Lmax)=117, repetition throughout the time series range.
- Trapping Time (TT)=22, very rare trapping in certain areas.

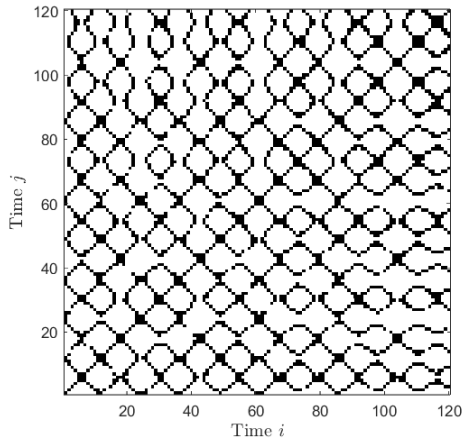

Figure 5: Recurrence plot of the tidal model forces during the first four months of 2025 (120 days in total).

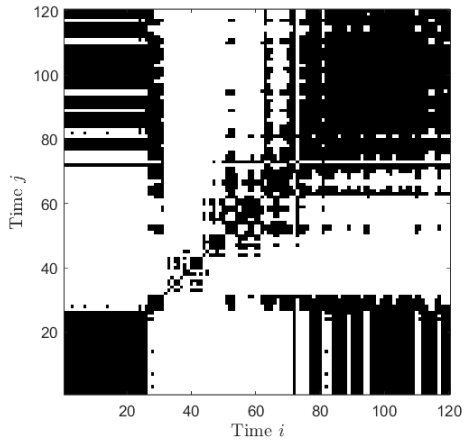

Figure 6: Recurrence plot of the earthquake daily rate during the first four months of 2025 (120 days in total).

The resulting JRP is illustrated in Fig. 7 and can be interpreted as follows:

1. *Dominant diagonal line (LOI)*: the prominent diagonal line indicates that both time series experience recurrences at similar time indices. This confirms temporal alignment between the series.
2. *Intermittent synchronization*: the density of recurrence points is low, indicating that the two systems have limited synchronized or joint dynamics (e.g., magnitude evolution and seismic rate driven by different mechanisms like fault stress vs. fluid movement).

By the RQA analysis we obtained

- Determinism (DET)=0.93, indicates that the two systems share strongly predictable, deterministic dynamics during the periods when they are both recurrent. This is a strong indicator of temporal correlation or phase synchronization.
- Laminarity (LAM)=0.69, indicates periods where both systems are "stuck" or evolve slowly in a synchronized manner. Can be linked to intermittent synchronization or common quasi-stationary behavior.
- Trapping Time (TT)=2.4, this low value suggests short-lived laminar phases, that is, the systems don't remain synchronized in stationary states for long.

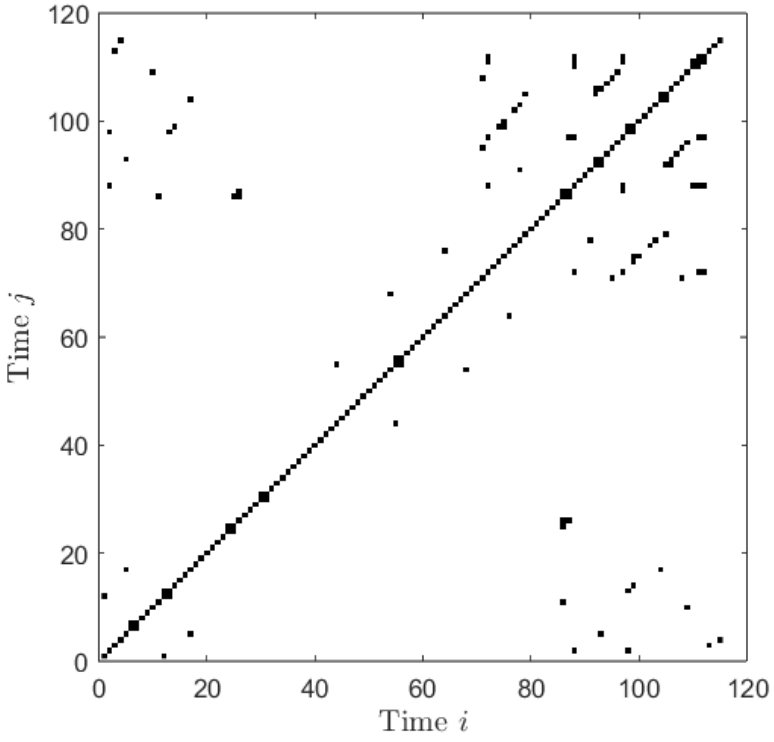

Figure 7: The joint recurrence plot (JRP) of the two time series shown in Fig. 8 where the numbering of time starts from 28^{th} day (0 corresponds to 28).

4 Investigation of causality

4.1 Granger causality method

A fundamental method for detecting causality in time series is the Granger Causality (GC) framework, which defines causality in terms of predictability [28], [29], [30], [31]. Specifically, a variable X is said to Granger-cause another variable Y if the inclusion of past values of X improves the prediction of Y beyond what is achievable using only past values of Y. This concept is mathematically formalized via linear auto-regressive models (AR), as shown below

$$Y_t = a_0 + \sum_{k=1}^{L} b_{1k} Y_{t-k} + \sum_{k=1}^{L} b_{2k} X_{t-k} + \xi_t. \tag{4.1}$$

where a_0 is constant, xi_t are uncorrelated random variables with zero mean and variance σ^2, L is the specified number of the time lags, and $t = L + 1...N$. The null hypothesis that "X_t does not Granger cause Y_t" is supported when $b_{2k} = 0$ for $k = 1, ..., L$ reducing to an expression without the presence of variable X_t. In this model, if the regression coefficients associated with past values of X are statistically significant, then X is considered to cause Y. The method is based on two key assumptions: a) the cause precedes the effect, and b) the cause contains unique information about the effect. GC has been widely used in disciplines such as economics, neuroscience, and climate science. It is effective for linear, stationary processes, but fails with nonlinearity, common in biological or chaotic systems. It cannot capture bidirectional or time-delayed nonlinear interactions well. Moreover, the GC respects the arrow of time and gives different results on time-reversed data, aligning with its assumption that causes precede effects.

4.2 Applying Granger causality test

In the context of investigating the causal relationship between tidal forces model (X) (cause) and the seismic activity of under study, that is, the earthquake daily rate (Y) (effect), we have implemented

the Granger causality method and its relevant Granger Test (GC). By using an appropriate software code, the obtained result is, p-value$= 0.034 < 0.05$, and thus, we reject the null hypothesis with a 5% significance level. Therefore, there is statistically significant evidence that the X time series causes the Y time series by Granger test. This means that there is strong relationship Granger causality, even with the data sample size used. Given that the Granger causality is effective mainly when the causal relationship is linear, we decided to proceed, in next, investigating also for a nonlinear one.

4.3 Convergent Cross Mapping implementation

The method of Convergent Cross Mapping (CCM) offers a fundamentally different approach tailored for nonlinear and chaotic dynamical systems. Rather than relying on predictability over time, CCM is based on the idea that if the time series X causes that of Y, then the historical states of Y will contain information about the states of X. It uses Taken's embedding theorem to reconstruct the state space of one system and check if it contains information about another system [32], [33]. For example, if Y contains information about X, then $X \to Y$ causality is inferred. It does this by forming delay vectors from one time series and using nearest neighbors to estimate the other. According to this method, we begin by forming the lagged-coordinate vectors

$$\underline{x}(t) = \langle X(t), X(t-\tau), X(t-2\tau), \ldots, X(t-(E-1)\tau) \rangle \tag{4.2}$$

where the range of t is, $t = 1 + (E-1)\,\tau$ to $t = L$ and τ the lag parameter.

This set of vectors is the "reconstructed manifold" or "shadow manifold" $\boldsymbol{M_X}$. Note that the term "shadow manifold" includes attractors defined on fractal sets. To generate a cross-mapped estimate of $Y(t)$, denoted by $\hat{Y}(t)|\boldsymbol{M_X}$, we begin by locating the contemporaneous lagged-coordinate vector on $\boldsymbol{M_X}$, $\underline{x}(t)$, and find its $E+1$ nearest neighbors. Note that $E+1$ is the minimum number of points needed for a bounding simplex in an E-dimensional space.

CCM is powerful for chaotic, nonlinear, deterministic systems, and has been successfully applied in ecology, climate dynamics, and physiology [34], [35], [36]. This approach does not rely on the assumption that the cause must temporally precede the effect, making it invariant under time reversal. Applying CCM to uni-directionally coupled systems, the inferred direction of causality remains the same even after reversing the time series. This characteristic underlines a key distinction between CCM and GC: while GC is sensitive to the temporal ordering of events, CCM evaluates the existence of shared dynamical structures regardless of direction in time. Therefore, although both methods aim to detect causal relationships, they operate under different conceptual frameworks and yield different insights, particularly in complex systems where temporal asymmetry is nontrivial.

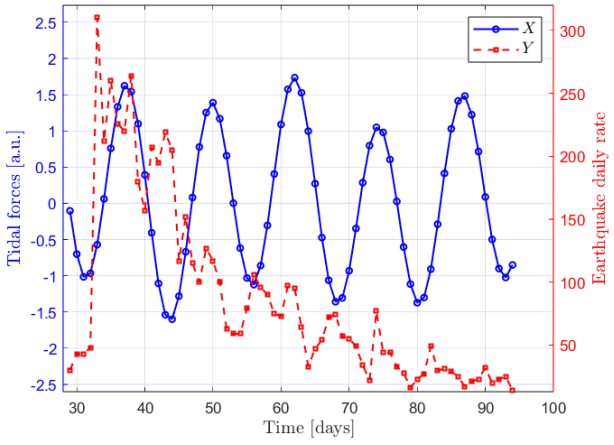

Figure 8: Plot of the investigated time series: tidal forces (X) and earthquake swarm daily rate (Y) from January 28 to April 30 during 2025 (93 days in total).

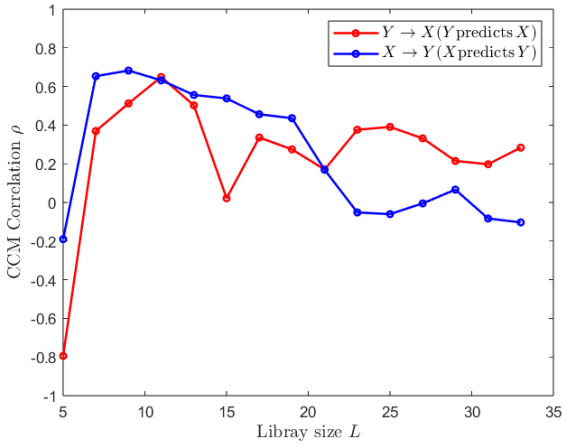

Figure 9: Plot of the obtained correlation coefficient ρ by applying the CCM method for the two potential cause and effect relationship $X \to Y$ and $Y \to X$.

For investigating a potential causal relationship between tidal forces and seismic triggering, and in turn driving the subsequent earthquake swarm long term activity, we calculated the daily rate of earthquakes during four months, January, February, March and April of 2025.

Until last days of February the earthquake daily rate was very low, of the order of 100, while by end of March began to gradually decrease at lower levels, around 30, and having the tendency to follow an exponential-type curve.

As the daily event rate was so very low, the corresponding magnitudes were also small, down to the mean level of $M_L 2.0$. Due to these low-magnitude events and their higher uncertainty, we selected the more characteristic and time period including the main seismic swarm, that is from January 28 to April 30, 2025. Namely, from the day 28 to day 120 of the year. For the same time period we considered the model of tidal forces including the combined Moon and Sun gravity interaction calculated for the particular region mentioned above. We must notice that the number of daily rate events (93) are close to the limit to be considered reliable for the CCM causality investigation. However, even if only marginally, we were able to obtain an understanding and justified result.

The CCM method has been implemented in a software code in Matlab including the investigation of the optimal time lag τ by using the mutual information algorithm between the two time series. The optimal value and used was $\tau = 3$. Additionally, the reasonable value $E = 2$ for the dimension of the embedded phase space system was used.

The Convergent Cross Mapping (CCM) method was applied to investigate the causal relationship between variables X (time series model representing the Lunar and Solar tidal forces superimposed) and Y (recorded earthquake daily rate, regardless of their Magnitude). In Fig. 8, the two investigated time series, tidal forces (X) and earthquake swarm daily rate (Y), are plotted within the selected time period, January 28 to March 31 during 2025. The result regarding the correlation coefficient ρ as a function of library size (L) in Fig. 9. The plot illustrates the ability of each variable to predict the other. Below we list the main findings of the analysis.

- support of the hypothesis of causal asymmetry: the CCM correlation coefficient ρ increases sharply as the library size grows from 5 to 7 and remains more or less stable mostly in direction ($X \to Y$ around the level of 0.53. Therefore, the higher correlation in the $X \to Y$ direction relative to $Y \to X$ indicates a predominantly unidirectional causal influence from X to Y.

- Stronger causal influence from X to Y: the $X \to Y$ direction exhibits higher and more stable correlations ($\rho \approx 0.6$) compared to the $Y \to X$ direction. Therefore, this picture suggests that variable X exerts a stronger causal effect on variable Y.

- Decline in predictive power for large library sizes: both curves show a noticeable drop in correlation for library sizes larger than approximately 17. This may be due to increased noise, rare events, or a limitation of CCM performance at large L values.

5 Evaluation of the results

5.1 Remarking results regarding causality

The obtained results have been based on three different methods, each of them having specific properties regarding their applicability to simple or complex dynamical systems described by two time series X and Y. Before proceeding with the evaluation, is useful to attribute an acronym for each method summarizing their basic features, as follows:

1. Joint Recurrence Plot (JRP): detects the occurrence of similar states and potential synchronization. If causality exists, it should be bidirectional, $X \longleftrightarrow Y$.

2. Granger Causality Test (GCT): appropriate for predictability identifying cause and effect in stochastic complex systems and exclusively for linear relationship and assumes time lag $\tau > 0$ for the effect. If causality exists, it should be unidirectional, that is, $X \to Y$.

3. Convergent Cross Mapping (CCM): appropriate for predictability identifying cause and effect in non linear or chaotic dynamical systems. If causality exists, it should be identified bidirectionally although a finite time lag $\tau > 0$ can help in discrimination, that is, $X \longleftrightarrow Y$.

Analysis Method	X, Y Synchronization	causality $X \to Y$
JRP	intermittent synchronization	–
GCT	–	p-value 0.034 (5% Significance Level)
CCM	–	$\rho_{\mathrm{XY,mean}} \approx 0.255$, $\rho_{\mathrm{YX,mean}} \approx 0.246$

Table 3: Summary of the overall and combined evaluation.

5.2 Global statistics of earthquake occurring

In the context of the present investigation, we considered it important to carry out a statistical study of strong earthquakes and beyond that have occurred during the last 50 years on our planet (from 1975 to 2025) with a chosen magnitude criterion (as a threshold). The relative uncertainty of the reported magnitudes variate between 0.4% and 0.7%.

Our aim was to calculate the percentage of an earthquake occurring within a time range around each of the four phases of the moon which expresses essentially a posterior probability. For this purpose, we collected earthquake data from USGS and we matched the day of the event with the Moon phase of the same day and at the corresponding location. This Earthquake Catalog provides real-time and historical earthquake information gathered from a global network of seismic monitoring stations [37]. The platform supports scientific analysis and public awareness by providing open-access, high-resolution earthquake data.

In this study we have used three different magnitude criterion, greater or equal than $M6.0$ (Strong and above), greater or equal than $M7.0$ (Major and above) and greater or equal than $M8.0$ (Great), The results are summarized in Tables 4, 5 and 6. The occurring percentage has been calculated by using two different ranges around each Moon phase, ± 4 (shown in the 1^{st} column, covering one quarter of the phase cycle) and ± 7 (shown in the 2^{nd} column, covering half phase cycle).

Moon phase	**Percentage** (range: ± 4 days) [%]	**Percentage** (range ± 7 days) [%]
New Moon	26.9	48.0
First Quarter	25.3	25.0
Full Moon	24.6	24.7
Last Quarter	23.2	2.3

Table 4: Percentages of earthquakes occurring within the four Moon phases. Number of events 7055. Magnitude criterion greater or equal than $M6.0$.

Moon phase	**Percentage** (range: ± 4 days) [%]	**Percentage** (range ± 7 days) [%]
New Moon	27.8	49.1
First Quarter	22.4	21.4
Full Moon	24.6	26.8
Last Quarter	25.2	2.7

Table 5: Percentages of earthquakes occurring within the four Moon phases. Number of events 695. Magnitude criterion greater or equal than $M7.0$.

Moreover, we have studied the statistics by using the criterion of greater or equal than $M8.0$ but extending the time period since the 1925, that is for 100 years ago, referring to 77 events. However, the ranking of the percentages remains similar.

For the case of global statistics of earthquakes of greater or equal than $M8.0$ we can go further determining the density distribution function around the phases of New Moon and Full Moon as

Moon phase	**Percentage** (range: ±4 days) [%]	**Percentage** (range ±7 days) [%]
New Moon	30.7	48.7
First Quarter	20.5	17.9
Full Moon	28.2	30.7
Last Quarter	20.5	2.6

Table 6: Percentages of earthquakes occurring within the four Moon phases. Number of events 39. Magnitude criterion greater or equal than $M8.0$.

follows: let us assume that the triggering probability in these two phase is expressed by a normal probability density function (p.d.f.). Then, the probabilities for the ranges of $a = 4$ and $b = 7$ days represent the integral (or cumulative) of the p.d.f. (with zero mean and unknown standard deviation σ) which is expressed by the error function. The ratio of the corresponding integrals, analytically, includes the two parameters, a and b, and the unknown σ, as follows

$$r = \frac{I_a}{I_b} = \frac{\frac{1}{\sqrt{2\pi}\sigma}\int_{-a}^{a} e^{-x^2/2\sigma^2}\mathrm{d}x}{\frac{1}{\sqrt{2\pi}\sigma}\int_{-b}^{b} e^{-x^2/2\sigma^2}\mathrm{d}x} = \frac{\mathrm{erf}\left(\frac{a}{\sqrt{2}\sigma}\right)}{\mathrm{erf}\left(\frac{b}{\sqrt{2}\sigma}\right)} \tag{5.1}$$

For the New Moon phase we have, $r = 30.7/48.7 = 0.6304$, within different limits, $\pm a$ and $\pm b$. By solving the equation 5.1 we determine σ.

The obtained result is $\sigma = 7.2$ days. For the Full Moon phase, where $r = 28.2/30.7 = 0.919$, we have obtained, $\sigma = 2.3$ days, that is, corresponding to a much more narrow p.d.f. of normal distribution. In both cases, the corresponding p.d.f., centralized at these two Moon phases, must be normalized to 0.487 and 30.7, respectively.

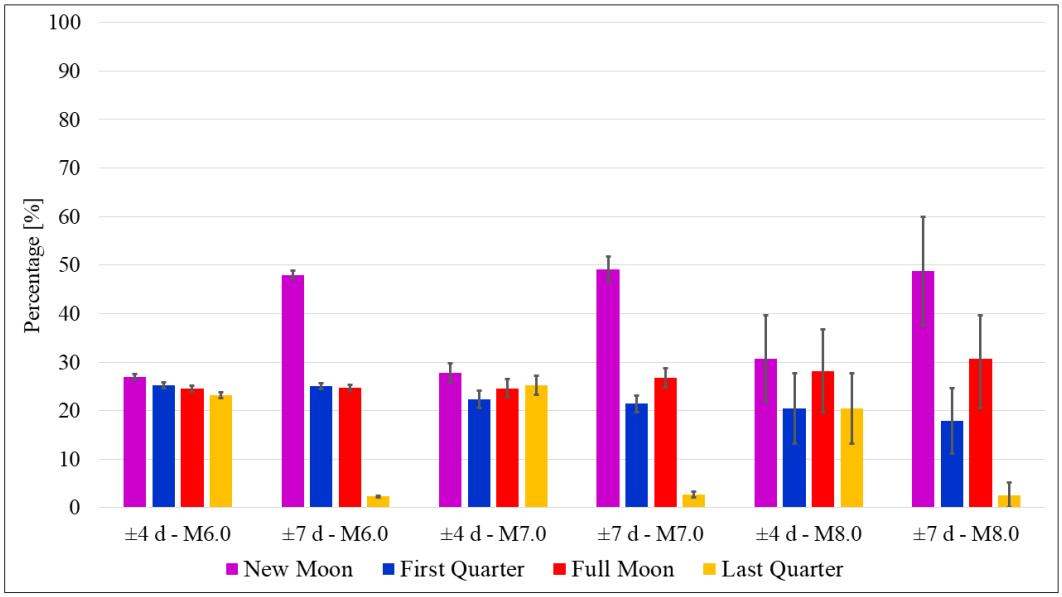

Figure 10: The overall earthquake occurring percentages during the various Moon phases. The tolerances in day and the magnitude thresholds are shown in each particular resulting group. The error bars represent the statistical errors. In the case of threshold $M8.0$, taking into account 100 year statistics, the statistical errors are reduced by about 30%.

Below, we enumerate the most important findings:

1. When the tolerance range increases from ±4 days to ±7 days the percentage of occurring in the New Moon phase increases. This demonstrates that the effect of this phase is broad, covering the whole range from First Quarter to Last Quarter phase.

2. As the criterion-threshold increases, the percentage for occurring in the New Moon phase increases.

3. For earthquakes of magnitude Major and beyond, about 60% of these occur in the region around the New Moon and Full Moon phase, while in the case of magnitude Great this reaches the impressive level of 80%.

4. The finding that the higher probability of tidal triggering concern strong earthquakes and beyond, must be due to the fact that the rupture of a long-length fault can be based on a cause when it is simultaneous as well as it extends along its entire length, as can happen through a tidal gravitational force interaction.

5. In the Last Quarter phase the obtained percentage of occurring is is extremely low compared to the others.

The overall results are presented in Fig. 10. The above statistical findings reinforce our study performed regarding the seismic swarm event in Greece alone.

5.3 Overall probability modeling and optimization

In the context of this global statistical study we present a modeling of an overall probability density function (p.d.f.) over each Moon phase cycle. This has been applied only for the threshold of $M8.0$ due to the possibility of extracting standard deviations. The assumptions we make are: a) the shape of each p.d.f. is normal function centered at the particular phase, b) the times (in days of a Moon phase cycle) of the four Moon phases are known - constants, $p_1 = d/2$, $p_2 = 3d/2$, $p_3 = 5d/2$ and $p_2 = 7d/2$ and c) the total p.d.f. will be the superposition of that of the individual phase. This function has the following form

$$f(x) = \sum_{i=1}^{4} \frac{c_i}{\sqrt{2\pi}\sigma_i} e^{-x^2/2\sigma_i^2} \tag{5.2}$$

where $i = 1$ corresponds to the New Moon phase.

According to our method, the periodic boundary condition, $f(0) = f(T) = f(4d) = f(29.53)$, where $T = 29.53$ days and $d = 7.3825$ days, must be hold, so that the probabilities at each consecutive Moon phase cycle should be conserved. The values of the maxima of the p.d.f. are taken equal to that obtained from the global statistics, $c_1 = 0.487$, $c_2 = 0.179$ $c_3 = 0.307$ and $c_4 = 0.026$, because of their normalization. The unknown parameters are, σ_1, σ_2, σ_3 and σ_4 and have to be determined by minimizing the function

$$\sum_{i=1}^{4} \frac{c_i}{\sqrt{2\pi}\sigma_i} \left(1 - e^{-(x-p_i)^2/2\sigma_i^2}\right) = 0 \tag{5.3}$$

To account for the infinite support of Gaussian functions and achieve periodic structure, the base function is extended over five consecutive periods, two before and two after that of reference, as follows

$$f_{\text{ext}}(x) = \sum_{k=-2}^{2} f(x + kT) \tag{5.4}$$

This ensures that boundary contributions from adjacent cycles are included when evaluating the central period. The standard deviations (σ_i) are optimized to minimize the endpoint discrepancy $|f(0) - f(T)|$. This condition enforces value-periodicity across cycles while allowing natural discontinuities in the derivative, avoiding artificial smoothness. The initial values were selected, $\sigma_{1,0} = 7.0$, $\sigma_{2,0} = 15$, $\sigma_{3,0} = 2.0$ and $\sigma_{4,0} = 15$. We notice that $\sigma_{2,0}$ and $\sigma_{4,0}$ must be greater than 12 due to low sensitivity of the objective function below them, otherwise the problem is characterized as overestimated presenting infinite solutions.

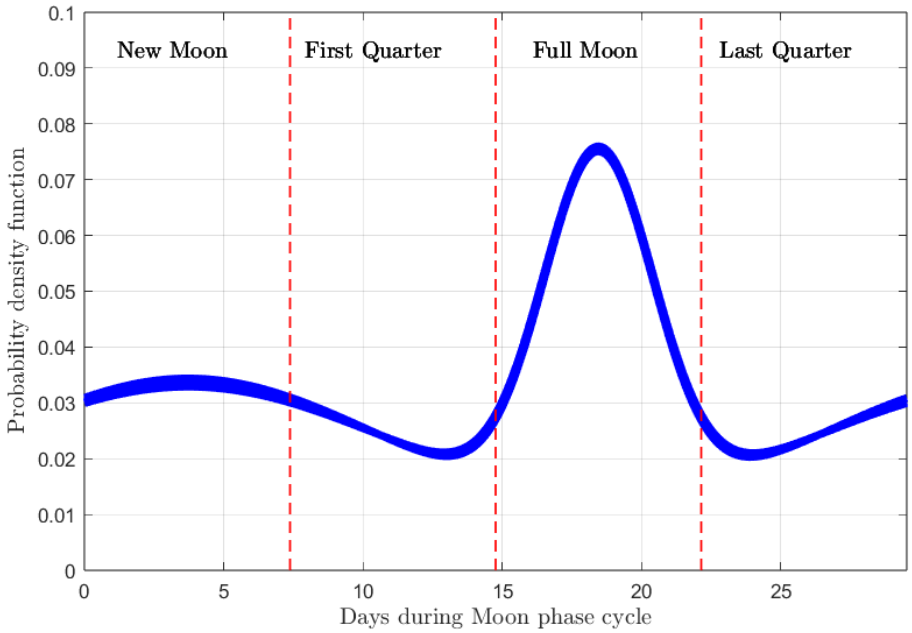

Figure 11: The overall p.d.f. during each Moon phase cycle, which ensures the continuity between the previous and next Moon phase. The p.d.f. of First Quarter and Last Quarter phases, due to their large time spread, overlap with the other two phases. The solid line width represents 1σ statistical uncertainty.

After performing the minimization, we have obtained the following values: $\sigma_1 = 7.503$, $\sigma_2 = 14.86$, $\sigma_3 = 1.992$ and $\sigma_4 = 14.54$ (all in units of days). The corresponding plot for the overall p.d.f. is shown in Fig. 11. The accomplished accuracy by the minimization procedure was, $|f(0) - f(T)| < 10^{-9}$, while the probability normalization has been also satisfied. Summarizing, the proposed methodology generates a smooth and periodic probability density function along the Moon phase cycle providing a clear overall picture. The probability for a specific symmetrical range of days around the four Moon phases can be calculated by numerical integration of this model by using the corresponding error functions (see Eq. 5.1).

Conclusions and Prospects

In this work we deeply studied the earthquake swarm occurred in the extended region between Santorini and Amorgos in Greece during the first months of 2025. Based on combined results obtained by using appropriate analysis methods, we have established a clear sign of causality between the tidal forces expressed by a simple model considering this earthquake swarm as a single event. However, this must be interpreted as a kind of "triggering" or "probability boost" to the existing subsurface network of faults. The causal relationship appears to be mostly linear according to the GC test. The investigation of causality through appropriate mathematical treatment applied on a short-term seismic swarm, lasting a few months, was a rare opportunity in terms of scientific interest for better understanding these events in the Seismology in the context of science of Geophysics.

Our investigation results regarding this particular seismic swarm, are in general, consistent with the global statistical findings of large number of strong earthquakes and greater. Namely, according to this study, a clear temporal correlation was found, mainly with the New Moon phase, with wide spread, and less around the Full Moon phase periods, with narrower spread. The creation of modeling of the overall probability gives a generic picture of the statistical findings in the higher threshold earthquake magnitudes. In our future plans, regarding in this general context, we intend to re-explore this particular earthquake swarm, as well as others around the world, by using more accurate Lunar ans Solar tidal force models.

Funding

This work was not funded.

Data availability statement

This manuscript has no associated data or the data will not be deposited.

Declarations

Conflict of interest

The author has declared that he has no conflict of interest with respect to this content.

Ethics

The author has declared ethics committee/IRB approval is not relevant to this content.

Acknowledgments

We gratefully thank Dr. V. Karastathis, Director of the Institute of Geodynamics of the National Observatory of Athens, for our discussions and for his valuable suggestions on the seismic data and other relevant issues in the context of geodynamics.

In this study, we used MATLAB, a high-level language developed by the Mathworks, Inc. Some parts of the codes and the initial syntax in some cases were generated by synergy with ChatGPT (OpenAI, 2025), (Version 4.0 retrieved from https://openai.com) and reviewed by the authors for precise scientific validity.

References

[1] M. Athanasopoulou, et. al, *Observations and Preliminary Results of the Seismic Sequence between Santorini and Amorgos*, 14-2-2025, Institute of Geodynamics – National Observatory of Athens, https://www.gein.noa.gr/.

[2] J. D. Griffin, M. W. Stirling, and T. Wang, *Periodicity and Clustering in the Long-Term Earthquake Record*, Geophysical Reasearch Letters,47, e2020GL089272, http://DOI 10.1029/2020GL089272, 2020.

[3] A. Saichev and D. Sornette, *Theory of earthquake recurrence times*, Journal of Geophysical Research, Vol. 112, B04313, doi:10.1029/2006JB004536, 2007.

[4] T. J. Ader, J. P. Avouac, *Detecting periodicities and declustering in earthquake catalogs using the Schuster spectrum, application to Himalayan seismicity*, Earth and Planetary Science Letters Volumes 377–378, September 2013, Pages 97-105.

[5] E. S. Cochran J. E. Vidale and S. Tanaka (2004), *Earth tides can trigger shallow thrust fault earthquakes*. Science, 306(5699), 1164–1166. https://doi.org/10.1126/science.1103961.

[6] L. Métivier, O. de Viron, C. P. Conrad, S. Renault, and M. Diament, G. Patau, (2009), *Evidence of earthquake triggering by the solid Earth tides*, Earth and Planetary Science Letters, 278(3–4), 370–375. https://doi:10.1016/j.epsl.2008.12.024.

[7] V. K. Karastathis, G. Eleftheriou, M. Kafatos et al. *Observations on the stress related variations of soil radon concentration in the Gulf of Corinth, Greece*, Sci Rep 12, 5442 (2022), https://doi.org/10.1038/s41598-022-09441-0.

[8] G. Sottili, D. Palladino, B. Giaccio, P. Messina, *Benford's Law in Time Series Analysis of Seismic Clusters*, Mathematical Geosciences, ISSN 1874-8961, http://DOI 10.1007/s11004-012-9398-1, 2012.

[9] A. Taushanov, *Seismic analysis based on Newcomb–Benford Law deviation estimation*, Progress in Engineering Science 2 (2025) 100051.

[10] T. Alexopoulos1, S. Leontsinis, *Benford's Law in Astronomy*, Indian Academy of Sciences, Astrophys. Astr. (2014) 35, 639–648.

[11] L. Pietronero, E. Tosatti, V. Tosatti, A. Vespignani, *Explaining the uneven distribution of numbers in nature: the laws of Benford and Zipf*, Physica A 293 (2001) 297–304.

[12] F. Benford,1938, *The law of anomalous numbers*, Proc. Am. Phil. Soc., 78, 551.

[13] N. M. Beeler, D A Lockner, *Why earthquakes correlate weakly with the solid Earth tides: effects of periodic stress on the rate and probability of earthquake occurrence*, J Geophys Res 108(B8):2391, doi:10.1029/2001JB001518.

[14] D. A. Lockner, N. M. Beeler (1999), *Premonitory slip and tidal triggering of earthquakes*, J Geophys Res 104(20):133–151.

[15] MATLAB R2024b, The MathWorks, Inc., Natick, Massachusetts, United States.

[16] G. D. Egbert and S. Y. Erofeeva, (2002). *Efficient inverse modeling of barotropic ocean tides*, Journal of Atmospheric and Oceanic Technology, 19(2), 183–204.

[17] Bruce B. Parker, *Tidal Analysis and Prediction*, Ph.D Thesis, Library of Congress Control Number: 2007925298, Silver Spring, Maryland July 2007.

[18] Institute of Geodynamics, National Observatory of Athens, General/Services, Database Search.

[19] N. Marwan, M. C. Romano, M. Thiel, J. Kurths, *Recurrence plots for the analysis of complex systems*, Physics Reports 438 (2007) 237 – 329.

[20] H. Poincaré, *Sur la probleme des trois corps et les équations de la dynamique*, Acta Mathematica 13 (1890) 1–271.

[21] J. P. Eckmann, S. O. Kamphorst, D. Ruelle, *Recurrence plots of dynamical systems*, Europhys. Lett. 5 (1987) 973–977.

[22] N. Marwan, N. Wessel, U. Meyerfeldt, A. Schirdewan, J. Kurths. *Recurrence-plot-based measures of complexity and their application to heart-rate-variability data*, Phys. Rev. E Stat. Nonlin. Soft Matter Phys. 2002 Aug;66(2 Pt 2):026702. doi: 10.1103/PhysRevE.66.026702. Epub 2002 Aug 6. PMID: 12241313.

[23] N Marwan, N. Schinkel, S. J. Kurths,(2013), *Recurrence plots 25 years later – Gaining confidence in dynamical transitions*, Europhys. Lett. 101, 20007p.

[24] T. Chelidze, T. Matcharashvili, *Complexity of seismic process; measuring and applications – A review*, Tectonophysics, 431(1–4), 49–60 (2007), DOI:10.1016/j.tecto.2006.05.029.

[25] D. Chorozoglou, E. Papadimitriou, *Investigation of earthquake recurrence networks: the cases of 2014 and 2015 aftershock sequences in Ionian Islands, Greece*, Natural Hazards, 102, 783–805 (2020). DOI:10.1007/s11069-020-03915-y.

[26] T. Chelidze, T. Matcharashvili, *Dynamical Patterns in Seismology, Recurrence Quantification Analysis – Theory and Best Practices*, Eds. C. L. Webber, Jr. and N. Marwan, Springer, Cham. 291-334 (2015), DOI:10.1007/978-3-319-07155-8-10.

[27] M. Lin, G. Zhao, G. Wang, *Recurrence quantification analysis for detecting dynamical changes in earthquake magnitude time series*, International Journal of Modern Physics C, 26(7), 1550077 (2015). DOI:10.1142/S0129183115500771.

[28] N. Wiener, *The theory of prediction in Modern Mathematics for the Engineer*, edited by E. F. Beckenbach (McGraw-Hill, New York, NY, 1956), pp. 125–139.

[29] C. W. J. Granger*Investigating Causal Relations by Econometric Models and Cross-spectral Methods*, Econometrica, Vol. 37, No. 3 (Aug., 1969), pp. 424-438, https://www.jstor.org/stable/1912791.

[30] C. W. J. Granger, *Time series analysis, cointegration, and applications*, Nobel Lecture, December 8, 2003, in Les Prix Nobel. The Nobel Prizes 2003, edited by T. Frängsmyr (Nobel Foundation, Stockholm, 2004), pp. 360–366.

[31] M. Paluš, A. Krakovská, J. Jakubík, M. Chvosteková, *Causality, dynamical systems and the arrow of time*, Chaos 1 July 2018; 28 (7): 075307.

[32] F. Takens, 1981, *Detecting strange attractors in turbulence. In Dynamical systems and turbulence*, Lecture notes in mathematics, ed. D.A. Rand and L.-S. Young, vol. 898, 366–381. New York: Springer-Verlag.

[33] G. Sugihara, et al. 2012. *Detecting causality in complex ecosystems*, Science 338: 496–500.

[34] A. A. Tsonis, E. R. Deyle, H. Ye, and G. Sugihara, *Convergent Cross Mapping: Theory and an Example*, Springer International Publishing AG 2018 A.A. Tsonis (ed.), Advances in Nonlinear Geosciences, DOI 10.1007/978-3-319-58895-727.

[35] S. Kacimi, and S. Laurens, *The correlation dimension: A robust chaotic feature for classifying acoustic emission signals generated in construction materials*, J. Appl. Phys. 106, 024909 (2009); doi.org/10.1063/1.3169601.

[36] J. Runge, *Causal network reconstruction from time series: From theoretical assumptions to practical estimation*,Chaos 1 July 2018; 28 (7): 075310. doi.org/10.1063/1.5025050.

[37] U. S. Geological Survey (USGS), Earthquake Catalog. U. S. Geological Survey, Link: earthquake.usgs.gov/earthquakes/search/. Accessed April 20, 2025.